

## CERTIFICATE

It is certified that the work contained in the thesis titled "Removal of Cadmium, Lead and Hexavalent Chromium from Wastewater" has been carried out under my supervision and that work has not been submitted elsewhere for a degree.

It is further certified that the student has fulfilled all the requirements of Comprehensive Examination, Candidacy and SOTA for the award of Ph.D. Degree.



**Dr. Vishal Mishra**

**(Supervisor)**

**School of Biochemical Engineering,**

**Indian Institute of Technology**

**(Banaras Hindu University)**

**Varanasi – 221005, India**

## DECLARATION BY THE CANDIDATE

I, **Veer Singh**, certify that the work embodied in this thesis is my own bona fide work and carried out by me under the supervision of "**Dr. Vishal Mishra**" from "**December, 2017**" to "**November, 2021**" at the "**School of Biochemical Engineering**", Indian Institute of Technology (BHU), Varanasi. The matter embodied in this thesis has not been submitted for the award of any other degree/diploma. I declare that I have faithfully acknowledged and given credits to the research workers wherever their works have been cited in my work in this thesis. I further declare that I have not wilfully copied any other's work, paragraphs, text, data, results, etc., reported in journals, books, magazines, reports dissertations, thesis, etc., or available at websites and have not included them in this thesis and have not cited as my own work.

Date : 5/11/2021

Signature of the Student

Place : IIT (BHU), Varanasi - 221005

(**Veer Singh**)

## CERTIFICATE BY THE SUPERVISOR

It is certified that the above statement made by the student is correct to the best of my knowledge.

Dr. Vishal Mishra

(Supervisor)

Coordinator of School

25/03/2022

समन्वयक  
Coordinator

जैव रासायनिक अभियांत्रिकी स्कूल  
School of Biochemical Engg  
भारतीय प्रौद्योगिकी संस्थान  
Indian Institute of Technology  
(काजहैदरगंज) वाराणसी-221005  
(B.H.U.) Varanasi

## COPYRIGHT TRANSFER CERTIFICATE

**Title of the Thesis:** "Removal of Cadmium, Lead and Hexavalent Chromium from Wastewater"

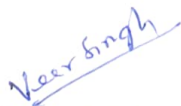
**Name of Student:** Veer Singh

### Copyright Transfer

The undersigned hereby assigns to the Indian Institute of Technology (Banaras Hindu University), Varanasi all rights under copyright that may exist in and for the above thesis submitted for the award of the Ph.D.

Date : 8/11/2021

Place : IIT (BHU), Varanasi

  
Mr. Veer Singh

(Student)

**Note:** However, the authors may reproduce or authorize others to reproduce material extracted verbatim from the thesis or derivative of the thesis for author's personal use provided that the source and the Indian Institute's copyright notice are indicated.

## Acknowledgements

- ❖ *Through this page, I offer my salutation, to the creator of this pious seat of learning Bharat Ratna Mahamana Pt. Madan Mohan Malviya Ji.*
- ❖ It is indeed my proud privilege to express my deep sense of gratitude and indebtedness to my supervisor, Dr. Vishal Mishra, Assistant Professor, School of Biochemical Engineering, Indian Institute of Technology (BHU), Varanasi for his immense help, cooperation and valuable guidance that he has extended to me for the successful completion of this investigation. I am grateful for his constant encouragement, sustained interest and parental care throughout the research period.
- ❖ I am obliged very much to express my sincere thanks to Coordinator, Prof. Vikas Kumar Dubey, School of Biochemical Engineering, Indian Institute of Technology (BHU) for providing necessary facilities and constant motivation throughout my research work.
- ❖ It is my privilege to express my thanks to all RPEC members Dr. Pradeep Kumar, Department of Chemical Engineering and Technology, IIT (BHU) and Prof. Vikas Kumar Dubey, School of Biochemical Engineering, IIT (BHU) for appropriate suggestions and kind cooperation.
- ❖ I am obliged very much to express my sincere thanks to all the faculty members, School of Biochemical Engineering, IIT (BHU) for their support and encouragement.
- ❖ I reserve special thanks for all the non-teaching staff of the School of Biochemical Engineering, IIT (BHU) as this work would have never been completed without their technical support
- ❖ I also gratefully acknowledge to the Ministry of Human Resource and Development (MHRD), Government of India, New Delhi, and Director, IIT (BHU) for the financial support in the form of teaching assistantship.

- ❖ My heartfelt thanks go to my dear labmates, I would like to special thanks to Jyoti Singh, Vishal Singh, Manisha Verma and Ashok Kumar Pal for their valuable support, encouragement towards the successful completion of my research work and making the journey happy.
- ❖ It's been possible with the blessings of my father, mother, brothers and sister that provided me all the wisdom, strength and guidance to carry on this journey which at times became very tough and tedious. Without their care, love, sacrifice, prayers, wishes, patience and motivation I can't even imagine of my present position in life.

## **Table of Contents**

<b>Contents</b>	<b>Page No.</b>
<b>Chapter 1: Introduction.....</b>	<b>1-10</b>
<b>Chapter 2: Literature of Review.....</b>	<b>11-41</b>
2.1 Heavy metal pollution: Source and toxicity.....	12
2.2 Removal of heavy metal ions.....	16
2.2.1 Biosorption.....	17
2.2.2 Bioaccumulation: Removal of heavy metal using living cells.....	28
2.2.2.1 Bacterial species: Role in bioremediation of heavy metal ions.....	28
2.2.2.3 Microbial reduction of Cr (VI).....	33
2.2.2.3 Mycoremediation: Fungal mediated removal of heavy metal ions.....	35
2.2.2.4 Heavy metal detoxification mechanism in living cells: Metal binding protein and antioxidant system.....	38
2.2.3 Modelling approaches for heavy metal biosorption.....	39
2.2.3.1 Adsorption kinetic study.....	39
2.2.3.2 Adsorption isotherm study.....	39
2.2.3.3 Thermodynamics study.....	40
2.2.3.4 Artificial Neural Network (ANN).....	40
2.2.3.5 Adsorption dynamics and diffusivity coefficients.....	41
2.3 Thesis Objectives.....	42

<b>Chapter 3: Materials and methods</b> .....	<b>43-69</b>
3.1 Collection of biological waste.....	44
3.2 Preparation of stock solutions.....	44
3.2.1 Chemicals and reagents.....	44
3.2.2 Preparation of biosorbent.....	44
3.2.2.1 RH and FeRH.....	44
3.2.2.2 Synthesis of CMNPs.....	45
3.2.2.3 Preparation of ChCLP.....	45
3.3 Characterization of synthesized biosorbents.....	46
3.4 Dimensionless numbers and Artificial neural network (ANN).....	47
3.4.1 Derivation of dimensionless number.....	47
3.4.2 ANN.....	49
3.5 Adsorption study.....	49
3.5.1 Adsorption of Cr (VI) using RH and FeRH.....	49
3.5.2 Adsorption of Cr (VI), Cd (II) and Pb (II) using CMNPs.....	49
3.5.3 Adsorption of Cr (VI), Cd (II), and Pb (II) using ChCLP.....	50
3.5.4 Determination of percentage removal and adsorption capacity.....	50
3.6.0 Isotherms, Kinetics, Thermodynamics and Mechanistic study.....	51
3.6.1 Isotherm models.....	51
3.6.2 Thermodynamic.....	54

3.6.3 Kinetics.....	54
3.6.4 Mechanistic study.....	55
3.7.0 Desorption of heavy metal ions: regeneration of biosorbent.....	57
3.8.0 Continuous column study.....	58
3.8.1 Parameters and design of packed bed column.....	58
3.9.0 Isolation of new bacterial strain from the site contaminated with coal mine effluents: characterization and heavy metal removal.....	59
3.9.1 Collection and physicochemical characterization of wastewater.....	59
3.9.2 Isolation of heavy metal tolerant bacteria.....	60
3.9.3 Genomic DNA isolation.....	60
3.9.4 16S rRNA gene sequencing and molecular identification.....	61
3.9.5 Effect of various parameters on the microbial growth.....	61
3.9.6 Analysis of antioxidants activity in heavy metal exposed bacterial isolate.....	62
3.9.7 Analysis of heavy metal removal.....	62
3.9.8 SEM and EDX analysis of bacterial isolate.....	62
3.10.0 Bioremediation of toxic metal ions from coal washery effluent (CWE) by <i>Pleurotus florida</i> .....	63
3.10.1 Collection and characterization of CWE.....	63
3.10.2 Collection and preparation of the substrate for mushroom cultivation.....	63
3.10.3 Experimental design for bioremediation of CWE.....	63
3.10.3.1 Spawn preparation.....	64
3.10.3.2 Bioremediation of CWE.....	64
3.10.4 Analysis of metallothionein concentration in <i>P. florida</i> fruit body grown in CWE containing substrate.....	65

3.10.5 Analysis of antioxidant enzymatic system in <i>P. florida</i> grown in CWE containing substrate.....	66
3.10.6 Growth modelling of <i>P. florida</i> in CWE.....	66
3.10.7 FTIR and SEM analysis of <i>P. florida</i> fruit body.....	67
3.10.8 Sample preparation for heavy metal analysis.....	68
3.10.9 Statistical data analysis.....	68
<b>Results and Discussion.....</b>	<b>70</b>
<b>Chapter 4: Development of a cost-effective, recyclable and viable metal ion doped adsorbent for simultaneous adsorption and reduction of toxic Cr (VI) ions.....</b>	<b>71-102</b>
4.1 Introduction.....	72
4.2 Characterization of FeRH and RH.....	73
4.2.1 SEM analysis.....	73
4.2.2 EDX analysis.....	74
4.2.3 FTIR.....	75
4.2.4 Proximate and ultimate analysis.....	76
4.2.5 pHpzc.....	77
4.2.6 BET surface area.....	78
4.3.0 Dimensionless numbers.....	79
4.4.0 ANN.....	80
4.5.0 Conformity of oxidation state.....	82
4.6.0 Proposed mechanism: surface protonation, adsorption and reduction.....	84
4.7.0 Adsorption study.....	84
4.7.1 Effect of process parameters.....	84
4.7.1.1 pH.....	84
4.7.1.2 Initial metal ion concentration.....	85

4.7.1.3 RH and FeRH dosage.....	86
4.7.1.4 Contact time.....	86
4.7.1.5 Temperature.....	87
4.7.1.6 Agitation speed.....	87
4.7.2.0 Isotherm study.....	87
4.7.3.0 Thermodynamics.....	92
4.7.4.0 Adsorption kinetics.....	94
4.7.5 Mechanistic study.....	95
4.8.0 Assessment of adsorption capacities.....	96
4.9.0 Recovery of FeRH.....	99
4.10.0 Techno-economic analysis.....	101
4.11.0 Conclusion.....	101
<b>Chapter 5: Synthesis of chitosan coated manganese dioxide nanoparticles (CMNPs) and its application in the removal of Cr (VI), Cd (II) and Pb (II) from wastewater.....</b>	<b>103-158</b>
5.1 Introduction.....	104
5.2.0 Characterization of CMNPs.....	105
5.2.1 FTIR analysis.....	105
5.2.2 HR-TEM.....	107
5.2.3 HR-SEM.....	108
5.2.4 EDX Analysis and Elemental mapping.....	109
5.2.5 CMNPs size measurement using dynamic light scattering (DLS).....	111
5.2.6 Zero point charge ( $pH_{zpc}$ ).....	112
5.2.7 Specific surface area.....	114
5.2.8 XPS analysis and determination of oxidation state of chromium.....	115
5.3.0 Biosorption study.....	117

5.3.1 Optimization of process parameters.....	117
5.3.2 Isotherm.....	122
5.3.3 Kinetics.....	132
5.3.4 Thermodynamics .....	137
5.3.5 Dimensionless number and diffusivity coefficients.....	142
5.4.0 ANN Modeling.....	143
5.5.0 Comparison of heavy metal removal capacity.....	152
5.6.0 Complete removal of heavy metal ions in series batch reactor system.....	154
5.7.0 Desorption of heavy metal ions and regeneration of CMNPs.....	154
5.8.0 Techno-economic analysis.....	157
5.9.0 Conclusion.....	157
<b>Chapter 6: Removal of Cd (II), Cr (VI) and Pb (II) by using chitosan coated <i>Citrus limetta</i> peels biomass in synthetic wastewater.....</b>	<b>159-207</b>
6.1 Introduction.....	160
6.2.0 Characterization of the ChCLP.....	162
6.2.1 Surface morphological of chitosan coated <i>Citrus limetta</i> peels biomass.....	162
6.2.2 Energy dispersive X- ray analysis and elemental mapping.....	163
6.2.3 Fourier transformation infra-red analysis.....	166
6.2.4 Determination of pH range through point zero charge.....	167
6.2.5 Atomic Force Microscopy.....	168
6.2.6 XPS.....	170
6.3.0 Adsorption study.....	172
6.3.1 Experimental parameter optimization.....	172
6.3.2 Isotherm.....	177

6.3.3 Thermodynamics.....	185
6.3.4 Adsorption kinetic.....	188
6.3.5 Adsorption Dynamics and diffusivity coefficients.....	192
6.3.6 ANN Modeling.....	193
6.4.0 Complete removal of heavy metal ions in series batch reactor system.....	202
6.5.0 Regeneration of chitosan coated ChCLP.....	203
6.6.0 Techno-economic analysis.....	205
6.7.0 Conclusion.....	206
<b>Chapter 7: Microbial Removal of Cr (VI), Pb (II) and Cd (II) by a New Bacterial Strain Isolated from the Site Contaminated with Coal Mine Effluents.....</b>	<b>208-243</b>
7.1 Introduction.....	209
7.2.0 Physico-chemical characterization of wastewater (Source of water collection.....	210
7.3.0 Characterization of bacterial isolate.....	212
7.3.1 16S rRNA gene sequencing.....	212
7.3.2 SEM and EDX analysis.....	214
7.3.3 XPS analysis.....	218
7.3.4 FTIR.....	220
7.4.0 Effect of pH and temperature.....	222
7.5.0 Bacterial growth in presence of heavy metal ions and in control.....	223
7.6.0 Heavy metal bioremediation mechanism.....	226
7.6.1 Expression of antioxidants.....	226
7.6.2 Heavy metal uptake dynamics.....	228
7.7.0 Heavy metal removal efficiency of <i>Microbacterium paraoxydans</i> strain VSVM IIT(BHU).....	229
7.8.0 ANN Modeling.....	233

7.9.0 Comparison of heavy metal removal efficiency.....	239
7.10.0 Conclusion.....	242
<b>Chapter 8: Bioremediation of toxic metal ions from coal washery effluent by <i>Pleurotus florida</i>.....</b>	<b>244-275</b>
8.1 Introduction.....	245
8.2.0 Physiochemical characterization of CWE.....	247
8.3.0 Bioaccumulation of heavy metals in the <i>P. florida</i> fruit bodies.....	249
8.4.0 Removal of heavy metals from substrate (paddy straw) using <i>P. florida</i> .....	254
8.5.0 Growth modelling of <i>P. florida</i> in CWE.....	256
8.5.1 Growth kinetics of <i>P. florida</i> in control and at various concentrations of CWE.....	257
8.6.0 Bioaccumulation mechanism of heavy metals in the <i>P. florida</i> .....	259
8.6.1 Metallothionein concentration in the <i>P. florida</i> .....	260
8.6.2 Antioxidant enzymatic system of <i>P. florida</i> .....	261
8.6.3 FTIR analysis of <i>P. florida</i> .....	265
8.7.0 SEM and EDX Analysis.....	268
8.8.0 Effect of initial heavy metal concentration including other wastewater components on the bioremediation efficiency and growth of <i>P. florida</i> .....	270
8.9.0 Comparison of removal efficiency in terms of heavy metal ions by <i>Pleurotus florida</i> and other fungal species.....	271
8.10 Conclusion.....	274
<b>Chapter 9.....</b>	<b>276-291</b>
9.1 Disposal of used adsorbent.....	277

9.2 Comparative heavy metal removal.....	277
9.3 Column study.....	278
9.4 Recommendations for future studies.....	281
9.5 Life cycle assessment theoretical study for the removal of Cadmium, Lead and Hexavalent Chromium from wastewater.....	282
9.5.1 Life Cycle Assessment (LCA) framework of the study.....	282
9.5.2 Aim and possibility description.....	285
9.5.3 Inventory study.....	285
9.5.4 Improvement evaluation.....	289
<b>Chapter 10. References.....</b>	<b>292-376</b>
<b>List of Publication.....</b>	<b>377-380</b>
<b>Conference/workshop.....</b>	<b>381</b>
<b>Research work under media coverage.....</b>	<b>382-384</b>

## List of Figures

<b>Figures</b>	<b>Captions</b>	<b>Page No.</b>
<b>Figure 2.1.</b>	Mechanism of heavy metal biosorption	17
<b>Figure 2.2</b>	Schematic representation of biosorbent preparation	19
<b>Figure 3.1</b>	Continuous fix bed column	59
<b>Figure 4.1</b>	SEM image of (a) unloaded RH (b) metal loaded RH (c) unloaded FeRH (d) metal loaded FeRH	73
<b>Figure 4.2</b>	EDX spectra of (a) unloaded RH (b) metal loaded RH (c) unloaded FeRH (d) metal loaded FeRH	74
<b>Figure 4.3</b>	FTIR spectra of (a) RH and FeRH (b) metal unloaded and loaded RH (c) metal unloaded and loaded FeRH	75
<b>Figure 4.4</b>	pH <sub>pzc</sub> value of FeRH	78
<b>Figure 4.5</b>	Performance plot of (a) RH and (b) FeRH	81
<b>Figure 4.6</b>	Comparison of predictive and experimental values for (c) RH and (d) FeRH using ANN	81
<b>Figure 4.7</b>	XPS analysis of Cr (VI) loaded FeRH	82
<b>Figure 4.8</b>	Oxidation state of adsorbed Cr on to FeRH	83
<b>Figure 4.9</b>	Effect of various adsorption parameters such as adsorbent dosage (a), initial Cr (VI) concentration (b), pH (c), agitation rate (d), temperature (e) and contact time (f) for Cr (VI) adsorption onto RH and FeRH.	85

<b>Figure 4.10</b>	Langmuir (a), Freundlich (b), Temkin (c), D-R (d), Halsey (e), H-R (f), Jovanovic (g) and R-P isotherm of Cr (VI) adsorption onto RH.	88
<b>Figure 4.11</b>	Langmuir (a), Freundlich (b), Temkin (c), D-R (d), Halsey (e), H-R (f), Jovanovic (g) and R-P isotherm of Cr (VI) adsorption onto FeRH.	89
<b>Figure 4.12</b>	Thermodynamic study of Cr (VI) adsorption onto RH and FeRH	93
<b>Figure 4.13</b>	PFO (a), PSO (b) and Elovich kinetic (c) of Cr (VI) adsorption of RH and FeRH	94
<b>Figure 4.14</b>	Diagrammatic representation of Cr (VI) removal	99
<b>Figure 4.15</b>	Sequences of Cr (VI) adsorption and desorption	100
<b>Figure 5.1</b>	FTIR spectra of chitosan, MNPs, CMNPs (a) and heavy metal loaded CMNPs (b)	106
<b>Figure 5.2</b>	Size and shape of CMNPs (a-b), lattice fringes indicated by arrows (c) and SAED pattern of CMNPs (d)	107
<b>Figure 5.3</b>	HR-SEM micrographs of CMNPs (a, b)	108
<b>Figure 5.4</b>	EDX analysis of CMNPs before (a) and after Cr (VI) (b), Cd (II) (c), Pb (II) (d) and ternary (e) metal ion biosorption	109-110
<b>Figure 5.5</b>	Elemental mapping of CMNPs after heavy metal biosorption. Elemental mapping representing distribution of all elements (a), carbon (b), nitrogen (c), oxygen (d), Pb (II) (e), Cd (II) (f), Cr (g) and Mn (h).	111
<b>Figure 5.6</b>	DLS analysis of CMNPs	112
<b>Figure 5.7</b>	pH <sub>zpc</sub> value of CMNPs	113

<b>Figure 5.8</b>	XPS of Cr (VI) (a), Cd (II) (b), Pb (II) (c) and ternary metal ion (d) biosorption on CMNPs.	115
<b>Figure 5.9</b>	Incidence of Cr (III) and Cr (VI) after reduction	116
<b>Figure 5.10</b>	Effect of pH (a), initial Cr (VI) concentration (b), CMNPs dosage (c), temperature (d), contact time (e), and agitation rate (f) on Cr (VI) removal using CMNPs	117
<b>Figure 5.11</b>	Effect of pH (a), initial Pb (II) concentration (b), CMNPs dosage (c), temperature (d), contact time (e) and agitation rate (f) for Pb (II) adsorption onto CMNPs	118
<b>Figure 5.12</b>	Effect of pH (a), initial Cd (II) concentration (b), CMNPs dosage (c), temperature (d), contact time (e), and agitation rate (f) on Cd (II) removal using CMNPs.	118
<b>Figure 5.13</b>	Langmuir (a), Freundlich (b), Temkin (c), and Halsey (d) isotherms of Cr (VI) biosorption CMNPs.	123
<b>Figure 5.14</b>	Langmuir (a), Freundlich (b), Temkin (c), and Halsey (d) isotherms of Pb (II) biosorption CMNPs.	124
<b>Figure 5.15</b>	Langmuir (a), Freundlich (b), Temkin (c), and Halsey (d) isotherms of Cd (II) biosorption on the surface of CMNPs.	124
<b>Figure 5.16</b>	Langmuir (a), Freundlich (b), Temkin (c), and Halsey (d) isotherms study of Cr (VI), Cd (II) and Pb (II) biosorption in ternary metal ion system onto CMNPs	125
<b>Figure 5.17</b>	PFO (a), PSO (b) and Elovich (c) kinetic models of Cr (VI) biosorption onto CMNPs.	132

<b>Figure 5.18</b>	PFO (a), PSO (b) and Elovich (c) kinetic models of Pb (II) biosorption onto CMNPs.	133
<b>Figure 5.19</b>	PFO (a), PSO (b) and Elovich (c) kinetics of Cd (II) biosorption onto CMNPs.	133
<b>Figure 5.20</b>	PFO (a), PSO (b), and Elovich (c) kinetics of Pb (II), Cd (II) and Cr (VI) biosorption in ternary metal ion system.	134
<b>Figure 5.21</b>	Thermodynamics of Cr (VI) (a), Pb (II) (b), Cd (II) (c) and ternary (d) metal ion system on to CMNPs.	137
<b>Figure 5.22</b>	Performance between number of epochs and the MSE for Cr (VI) ions in single metal system.	144
<b>Figure 5.23</b>	Performance between number of epochs and the MSE for Cd (II) ions in single metal ion system.	144
<b>Figure 5.24</b>	Performance between number of epochs and the MSE for lead ions in single metal ion system	145
<b>Figure 5.25</b>	Performance between number of epochs and the MSE for ternary metal ion system	145
<b>Figure 5.26</b>	Regression plot for Cr (VI) ions in single metal ion system	146
<b>Figure 5.27</b>	Regression plot for Cd (II) in single metal ion system	147
<b>Figure 5.28</b>	Regression plot for Pb (II) in single metal ion system	147
<b>Figure 5.29</b>	Regression plot for ternary metal ion system	148
<b>Figure 5.30</b>	Correlation plot for the experimental and ANN predicted values for Cr (VI) ions in single metal ion system	149
<b>Figure 5.31</b>	Correlation plot for the experimental and ANN predicted values for Cd (II) ions in single metal ion system	149

<b>Figure 5.32</b>	Correlation plot for the experimental and ANN predicted values for Pb (II) ions in single metal ion system	150
<b>Figure 5.33</b>	Correlation plot for the experimental and ANN predicted values for ternary metal ion system	150
<b>Figure 5.34</b>	Diagrammatic demonstration of heavy metal removal in series batch reactor system	154
<b>Figure 5.35</b>	Cr (VI) adsorption - desorption on CMNPs	155
<b>Figure 5.36</b>	Pb (II) adsorption - desorption on CMNPs	155
<b>Figure 5.37</b>	Cd (II) adsorption - desorption on CMNPs	156
<b>Figure 6.1</b>	SEM image of CLP (a), ChCLP (b), ChCLP-Cr(VI) (c), ChCLP-Pb (d), ChCLP-Cd(II) (e) and ChCLP-Cr(VI)-Cd(II)-Pb(II) (f).	162
<b>Figure 6.2</b>	The EDX analysis of selected spectrum area of ChCLP-Cr (VI) (a), ChCLP-Pb(II) (b), ChCLP-Cd(II) (c) and ChCLP-Cr(VI)-Pb(II)-Cd(II) (d).	164
<b>Figure 6.3</b>	Elemental mapping of C (a), N (b), O (c), Pb (d), Cd (e), Cr (f) and percentage wise distribution of all ternary metal ions including C, N and O (g).	165
<b>Figure 6.4</b>	FTIR spectra of CLP, chitosan, ChCLP and ChCLP-Cr (VI), ChCLP-Cd (II), ChCLP-Pb (II) in single and ternary metal ion system.	166
<b>Figure 6.5</b>	pH value at point zero charge ( $pH_{pzc}$ ) of ChCLP	167
<b>Figure 6.6</b>	AFM image of CLP in 2-D (a) and 3-D (b, c). AFM images of ChCLP in 2-D (d) and 3-D (e, f).	169
<b>Figure 6.7</b>	XPS spectra of ChCLP-Cr (VI) (a), ChCLP-Pb(II) (b), ChCLP-Cd(II) (c) of single and ternary (d) metal ion system.	170

<b>Figure 6.8</b>	Biotransformation of Cr (VI) into Cr (III) on ChCLP	171
<b>Figure 6.9</b>	Effect of pH (a), ChCLP dosage (b), initial Cr (VI) concentration (c) reaction temperature (d), contact time (e) and agitation rate (f) on the Cr (VI) removal	172
<b>Figure 6.10</b>	Effect of pH (a), ChCLP dosage (b), initial Cd (II) concentration (c), temperature (d), contact time (e), and agitation rate (f) on removal of Cd (II).	173
<b>Figure 6.11</b>	Effect of pH (a), ChCLP dosage (b), initial Pb (II) concentration (c), temperature (d), contact time (e), and agitation rate (f) on removal of Cd (II).	173
<b>Figure 6.12</b>	Langmuir (a) and Freundlich (b), Temkin (c) and Halsey (d) isotherm for Cr (VI) adsorption on ChCLP	178
<b>Figure 6.13</b>	Langmuir (a) and Freundlich (b), Temkin (c) and Halsey (d) isotherm for Pb (II) adsorption on ChCLP	178
<b>Figure 6.14</b>	Langmuir (a) and Freundlich (b), Temkin (c) and Halsey (d) isotherm for Cd (II) adsorption on ChCLP	179
<b>Figure 6.15</b>	Langmuir (a) and Freundlich (b), Temkin (c) and Halsey (d) isotherm for adsorption of Pb (II), Cd (II) and Cr (VI) in ternary metal ion system on ChCLP	179
<b>Figure 6.16</b>	Thermodynamics of Pb (II) (a), Cd (II) (b), Cr (VI) (c) adsorption in single and ternary (d) metal ions system on ChCLP	186
<b>Figure 6.17</b>	PFO (a) and PSO (b) and Elovich (c) kinetic model for Cr (VI) adsorption on ChCLP in single metal ion system	189
<b>Figure 6.18</b>	PFO (a) and PSO (b) and Elovich (c) kinetic model for Pb (II) adsorption on ChCLP in single metal ion system	189

<b>Figure 6.19</b>	PFO (a) and PSO (b) and Elovich (c) kinetic model for Cd (II) adsorption on ChCLP in single metal ion system	190
<b>Figure 6.20</b>	PFO (a) and PSO (b) and Elovich (c) kinetic model for adsorption of Cr (VI), Cd (II) and Pb (II) in ternary metal ion system on ChCLP	190
<b>Figure 6.21</b>	Performance between number of epochs and the MSE for Cr (VI) ions in single metal system	194
<b>Figure 6.22</b>	Performance between number of epochs and the MSE for Cd (II) ions in single metal ion system	194
<b>Figure 6.23</b>	Performance between number of epochs and the MSE for Pb (II) ions in single metal ion system	195
<b>Figure 6.24</b>	Performance between number of epochs and the MSE for ternary metal ion system	195
<b>Figure 6.25</b>	Regression plot for Cr (VI) ions in single metal ion system	196
<b>Figure 6.26</b>	Regression plot for Cd (II) ions in single metal ion system	197
<b>Figure 6.27</b>	Regression plot for Pb (II) ions in single metal ion system	197
<b>Figure 6.28</b>	Regression plot for ternary metal ion system	198
<b>Figure 6.29</b>	Correlation plot for the experimental and ANN predicted values for Cr (VI) ions in single metal ion system	199
<b>Figure 6.30</b>	Correlation plot for the experimental and ANN predicted values for Cd (II) ions in single metal ion system	199
<b>Figure 6.31</b>	Correlation plot for the experimental and ANN predicted values for Pb (II) ions in single metal ion system	200
<b>Figure 6.32</b>	Correlation plot for the experimental and ANN predicted values for ternary metal system	200

<b>Figure 6.33</b>	Diagrammatic demonstration of heavy metal removal in series batch reactor system	202
<b>Figure 6.34</b>	Adsorption and desorption of Cr (VI) on ChCLP	203
<b>Figure 6.35</b>	Adsorption and desorption of Cd (II) on ChCLP	204
<b>Figure 6.36</b>	Adsorption and desorption of Pb (II) on ChCLP	204
<b>Figure 7.1</b>	Gel electrophoresis image of amplified 16S rRNA gene of isolated bacteria	212
<b>Figure 7.2</b>	Phylogenetic tree of <i>Microbacterium paraoxydans</i> strain VSVM IIT (BHU) (accession number (MN650647). The analysis includes 18 nucleotide sequence.	213
<b>Figure 7.3</b>	SEM of bacterial isolate of control (a), Cr (VI) (b), Cd (II) (c), Pb (II) (d) exposed in single and exposed in ternary metal ion system.	215
<b>Figure 7.4</b>	EDX analysis of control (a), and Cr (VI) (b), Pb (II) (c), Cd (II) (d) and ternary metal ion (e) exposed <i>Microbacterium paraoxydans</i> strain VSVM IIT(BHU)	216-217
<b>Figure 7.5</b>	XPS analysis of control (a), Cr (VI) (b), Pb (II) (c) and Cd (II) (d) exposed <i>Microbacterium paraoxydans</i> strain VSVM IIT(BHU)	219
<b>Figure 7.6</b>	XPS spectra of <i>Microbacterium paraoxydans</i> strain VSVM IIT(BHU) after exposed simultaneous in ternary metal ion system of Cr (VI), Cd (II) and Pb (II).	220
<b>Figure 7.7</b>	FTIR spectra of Pb (II) and control (a), Cd (II) and control (b), Cr (VI) and control (c), and ternary metal ions (d).	221

<b>Figure 7.8</b>	Effect of pH (a) and temperature (b) on the growth of the isolated <i>Microbacterium paraoxydans</i> strain VSVM IIT(BHU).	222
<b>Figure 7.9</b>	Effect of heavy metal on growth of <i>Microbacterium paraoxydans</i> strain VSVM IIT(BHU) at heavy metal concentration of 100 mg/L (a) and 200 mg/L (b).	223
<b>Figure 7.10</b>	Effect of ternary heavy metal ions on bacterial growth	224
<b>Figure 7.11</b>	Antioxidant enzymatic activity in the <i>Microbacterium paraoxydans</i> strain VSVM IIT(BHU) grown in Cr (VI) (a), Pb (II) (b), Cd (II) (c) and ternary metal ions (d).	227
<b>Figure 7.12</b>	Heavy metal removal efficiency of <i>Microbacterium paraoxydans</i> strain VSVM IIT(BHU) in Cr (VI) (a), Pb (II) (b), Cd (II) (c) and ternary metal ion system of Cr (VI), Cd (II) and Pb (II) (d).	230
<b>Figure 7.13</b>	Performance between number of epochs and the MSE for Cr (VI) (a), Cd (II) (b), Pb (II) (c) ions in single metal system and ternary metal ion system (d).	233
<b>Figure 7.14</b>	Regression plot for Cr (VI) ions in single ion system	234
<b>Figure 7.15</b>	Regression plot for Cd (II) metal ion system	235
<b>Figure 7.16</b>	Regression plot for Pb (II) in single metal ion system	235
<b>Figure 7.17</b>	Regression plot for ternary metal ion system	236
<b>Figure 7.18</b>	Correlation plot for the experimental and ANN predicted values for Cr (VI) ions in single metal ion system	237
<b>Figure 7.19</b>	Correlation plot for the experimental and ANN predicted values for Cd (II) ions in single metal ion system	237

<b>Figure 7.20</b>	Correlation plot for the experimental and ANN predicted values for Pb (II) in single metal ion system	238
<b>Figure 7.21</b>	Correlation plot for the experimental and ANN predicted values for ternary metal ion system	238
<b>Figure 8.1a</b>	Pb (II) concentration in the mushroom fruit body grown in paddy straw substrate containing different concentration of CWE at various interval of time	249
<b>Figure 8.1b</b>	Cr concentration in the mushroom fruit body grown in paddy straw substrate containing different concentration of CWE at various interval of time	250
<b>Figure 8.1c</b>	Cd concentration in the mushroom fruit body grown in paddy straw substrate containing different concentration of CWE at various interval of time	250
<b>Figure 8.1d</b>	Zn concentration in the mushroom fruit body grown in paddy straw substrate containing different concentration of CWE at various interval of time	251
<b>Figure 8.1e</b>	As concentration in the mushroom fruit body grown in paddy straw substrate containing different concentration of CWE at various interval of time	251
<b>Figure 8.1f</b>	Mn concentration in the mushroom fruit body grown in paddy straw substrate containing different concentration of CWE at various interval of time	252
<b>Figure 8.1g</b>	Ni concentration in the mushroom fruit body grown in paddy straw substrate containing different concentration of CWE at various interval of time	252

<b>Figure 8.1h</b>	Cr concentration in the mushroom fruit body grown in paddy straw substrate containing different concentration of CWE at various interval of time	253
<b>Figure 8.2</b>	Metallothionein concentration in the mushroom grown in the various dilutions of CWE containing medium at several interval of time	260
<b>Figure 8.3a</b>	Superoxide dismutase (SOD) concentration in the mushroom grown in the various dilutions of CWE containing medium at several interval of time	262
<b>Figure 8.3b</b>	Glutathione concentration in the mushroom grown in the various dilutions of CWE containing medium at several interval of time	262
<b>Figure 8.3c</b>	Lipid Peroxidase concentration in the mushroom grown in the various dilutions of CWE containing medium at several interval of time	263
<b>Figure 8.3d</b>	Catalase concentration in the mushroom grown in the various dilutions of CWE containing medium at several interval of time	263
<b>Figure 8.4</b>	Schematic diagram representing the FTIR analysis of <i>P. florida</i> grown in control (a) and CWE containing substrate (b)	266-267
<b>Figure 8.5</b>	SEM micrograph cultivated in control and SEM micrograph (e-h) of <i>P. florida</i> (cultivated in CWE).	268
<b>Figure 8.6</b>	EDX spectra of <i>P. florida</i> mushroom.	269
<b>Figure 8.7</b>	Growth of <i>P. florida</i> (A-E) in the control and 100% CWE containing paddy straw	270
<b>Figure 9.1</b>	Breakthrough curve of Cr (VI) removal at flow rate 10, 20 and 30 ml/min	279

<b>Figure 9.2</b>	Breakthrough curve of Cd (II) removal at flow rate 10, 20 and 30 ml/min	279
<b>Figure 9.3</b>	Breakthrough curve of Pb (II) removal at flow rate 10, 20 and 30 ml/min	280
<b>Figure 9.4</b>	System boundary describing life cycle of production, use and recycle of the biosorbent corresponds to Cr (VI), Cd (II) and Pb (II) removal for contaminated wastewater system	282
<b>Figure 9.5</b>	Life cycle assessment four stages procedure	285

## List of Tables

<b>Table</b>	<b>Title</b>	<b>Page No.</b>
<b>Table 1.1</b>	The advantage and limitations of the heavy metal removal method	5-6
<b>Table 2.1</b>	Maximum limit of Cr (VI), Cd (II) and Pb (II) in the industrial effluent.	13
<b>Table 2.2</b>	The maximum permissible limit of Cr (VI), Cd (II) and Pb (II)	14
<b>Table 2.3</b>	Cr (VI) biosorption capacity of different biosorbent derived from algal, fungal, plants, bacterial biomass.	20-22
<b>Table 2.4</b>	Cd (II) biosorption capacity of different biosorbent derived from algal, fungal, plants, bacterial biomass.	22-24
<b>Table 2.5</b>	Pb (II) biosorption capacity of different biosorbents	24-25
<b>Table 2.6</b>	Nanomaterials and their heavy metal adsorption capacity	26-28
<b>Table 2.7</b>	Bacterial species and their Cr (VI) efficiency.	29-30
<b>Table 2.8</b>	Pb (II) removal efficiency of bacterial strains.	30-32
<b>Table 2.9</b>	Cd (II) removal efficiency of bacterial strains.	32-33
<b>Table 2.10</b>	Fungi and their heavy metal removal capacities	35-37
<b>Table 4.1</b>	Proximate and ultimate analysis of FeRH	76-77
<b>Table 4.2</b>	Specific surface area of FeRH, RH and other adsorbents	79
<b>Table 4.3</b>	Dimensionless numbers for RH and FeRH	80
<b>Table 4.4</b>	Isotherms parameters and constants	90-91
<b>Table 4.5</b>	Thermodynamic parameters	93-94
<b>Table 4.6</b>	Kinetic model constants and error functions	94-95

<b>Table 4.7</b>	Mechanistic parameters	95-96
<b>Table 4.8</b>	Cr (VI) uptake capacities of RH and FeRH and other adsorbents.	97-98
<b>Table 5.1</b>	Specific surface area of CMNPs and other nanoparticles	114
<b>Table 5.2</b>	Isotherms parameters of Cr (VI) biosorption on CMNPs	125-126
<b>Table 5.3</b>	The isotherm parameters of Pb (II) biosorption at various temperature	126-127
<b>Table 5.4</b>	The isotherm parameters of Cd (II) biosorption	127
<b>Table 5.5</b>	Isotherm parameters of Cr (VI), Cd (II) and Pb (II) biosorption in ternary metal ion system	128-130
<b>Table 5.6</b>	Kinetics of Cr (VI) biosorption	134
<b>Table 5.7</b>	Kinetics of Pb (II) biosorption	134
<b>Table 5.8</b>	Kinetic of Cd (II) biosorption on to CMNPs	134-135
<b>Table 5.9</b>	Kinetic parameters of Pb (II), Cd (II) and Cr (VI) biosorption in ternary metal ion system	135
<b>Table 5.10</b>	Thermodynamic data for biosorption of Cr (VI) on to CMNPs	137-138
<b>Table 5.11</b>	Thermodynamic data for biosorption of Pb (II) on to CMNPs	138
<b>Table 5.12</b>	Thermodynamic data for biosorption of Cd (II) on to CMNPs	138
<b>Table 5.13</b>	Thermodynamic parameters of Pb (II), Cd (II) and Cr (VI) biosorption on to CMNPs in ternary metal ion system	138-139
<b>Table 5.14</b>	Comparative thermodynamics data present study and literature	139-141
<b>Table 5.15</b>	Dimensionless numbers and diffusivity coefficients for heavy metal ions in single and ternary metal ion system.	142
<b>Table 5.16</b>	Comparison of heavy metal removal capacity of CMNPs with other nanoparticles	152-153

<b>Table 6.1</b>	Isotherm parameters of Cr (VI), Cd (II) and Pb (II) adsorption in single metal ion system	180-182
<b>Table 6.2</b>	The isotherm parameters of Cr (VI), Cd (II) and Pb (II) in the ternary metal ion system.	182-184
<b>Table 6.3</b>	Thermodynamic parameters of Cr (VI), Cd (II) and Pb (II) on ChCLP in single metal ion system.	186-187
<b>Table 6.4</b>	Thermodynamic parameters for adsorption of ternary metal ion system	187
<b>Table 6.5</b>	Kinetic parameters of Cr (VI), Cd (II) and Pb (II) adsorption on ChCLP in single metal ion system	190-191
<b>Table 6.6</b>	Kinetic parameters of heavy metal adsorption in ternary metal ion system.	191
<b>Table 6.7</b>	Value of dimensionless numbers and diffusivity coefficients for metal ions in single and ternary metal ion system.	192
<b>Table 7.1</b>	Physico-chemical characterization of wastewater	211
<b>Table 7.2</b>	Value of dimensionless numbers for metal ions in single and ternary metal ion system	229
<b>Table 7.3</b>	Comparison of heavy metal removal efficiency	239-241
<b>Table 8.1</b>	Characterization of CWE	247-248
<b>Table 8.2</b>	Metals present in paddy straw ( $\mu\text{g/g}$ ) before and after bioremediation	255
<b>Table 8.3</b>	Growth of <i>P. florida</i> in various concentration of CWE	257
<b>Table 8.4</b>	Study of exponential and linear growth models of <i>P. florida</i> in varying environmental conditions.	258

<b>Table 8.5</b>	Functional groups present in the <i>P. florida</i> (before and after bioremediation)	265-266
<b>Table 8.6</b>	Heavy metal removal efficiency of <i>P. florida</i> and other fungal species	271-274
<b>Table 9.1</b>	Comparative heavy metal removal capacity	277-278
<b>Table 9.2</b>	Heavy metals and its hazardous impact on community health	286-288

## Symbols and Abbreviations

mM	milli mole
$q_e$	uptake Capacity
$C_i$	Initial Cr (VI) concentration
$C_e$	Equilibrium Cr (VI) concentration
mL	Millilitre
mg	Milligram
L	Litre
t	Time
$C_a$	Heavy metal ion concentration in the desorbed solution
$V_a$	Desorbed solution volume
PFO	Pseudo first order kinetics
PSO	Pseudo second order kinetics
ASTDR	Agency for toxic substances and disease registry
CLP	<i>Citrus limetta</i> peels
ChCLP	Chitosan coated <i>Citrus limetta</i> peels
SEM	Scanning electron microscopy
EDX	Energy dispersive X- ray analysis
XPS	X-ray photoelectron spectroscopic
AFM	Atomic force microscopy
FTIR	Fourier transformation infra-red
ICP-OES	Inductively coupled plasma optical emission spectrometry
Cr (VI)	Hexavalent chromium
Cr (III)	Trivalent chromium

Cd (II)	Cadmium
Pb (II)	Lead
V	Volume
W	Weight
$r_0$	Radius of adsorbent
$\delta$	Thickness of film
D	Diffusion coefficient
R or r	Spherical radial coordinate
$\phi_b$	Adsorption flux
$\phi_d$	Desorption flux
S	Surface ligands
$C_s$	Subsurface ligands
$C^*$	Dimensionless concentration
$C$	Bulk concentration
$C_0$	Initial bulk concentration
$\zeta$	Dimensionless distance
$r_s$	Drop radius
$S^*$	Dimensionless surface concentration
$S_\infty$	Maximum surface concentration
$\tau$	Dimensionless time
k	Ratio of the surface concentration at equilibrium to bulk concentration
n	number of experiments
$q_t$	Biosorption or adsorption capacity at time $t$
$k_s$	Equilibrium rate constant

$k'_2$	Equilibrium constant
$a$	Initial biosorption rate
$\beta$	Extent of surface coverage
$Q^0$	Maximum uptake capacity
$b$	Langmuir isotherm constant
$k_f$ and $n$	Freundlich isotherm and affinity constants
$R$	Universal gas constant
$T$	Temperature
$A_T$	Temkin isotherm constant related to heat adsorption
$b_T$	Temkin isotherm constant related to the maximum binding energy
$K_H$ and $n_H$	Halsey isotherm constants
$\theta$	Degree of surface coverage
$n_{FH}$	number of ions occupying adsorption sites
$K_{FH}$	F-H equilibrium constant
$\Delta G^0$	Gibbs free energy
$\Delta H^0$	Enthalpy change
$\Delta S^0$	Entropy change
$q_H$	Maximum uptake capacity of Hill isotherm
$K_D$ , and $n_H$	Hill isotherm constants
$RH$	rice husk
$FeRH$	Ferrous ion coated rice husk
$CMNPs$	Chitosan coated $MnO_2$ nanoparticles
$Al$	Aluminium
$As$	Arsenic

Co	Cobalt
Cu	Copper
Mn	Manganese
Fe	Iron
Ni	Nickel
APHA	American Public Health Association
BOD	Biological oxygen demand
CWE	Coal washery effluent
EDTA	Ethylenediaminetetraacetic acid
$A$	Growth rate
$K_r$	Growth per day
$B$	Growth at time $t$
$\beta_0$	Growth at time $t=0$
Cm	Centimetre
$\mu\text{l}$	Microliter
M	Molar
Nm	Nanometer
HNO <sub>3</sub>	Nitric acid
HClO <sub>4</sub>	Perchloric acid
PBS	Phosphate saline buffer
PDA	Potato dextrose agar
KBr	Potassium bromide
ROS	Reactive oxygen species
GSH	Reduced glutathione

Rpm	Revolution per minute
SDS	Sodium dodecyl sulphate
SOD	Superoxide peroxidase
H <sub>2</sub> SO <sub>4</sub>	Sulphuric acid
USEPA	United States Environmental Protection Agency
WHO	World Health Organization

## **Preface**

The heavy metal ions like hexavalent chromium, cadmium, lead, arsenic, nickel are well-known carcinogens that amalgamate in the effluent of leather/ tanning industry, textile dyeing production, electroplating and rubber manufacturing plant, chrome plating and coal washery unit. The removal of heavy metal ions from contaminated water is necessary due to their toxicity. Various conventional methods such as membrane filtration, chemical precipitation, electro-dialysis, reverse osmosis and electrochemical precipitation have been used for the removal of toxic metal ions from domestic and industrial wastewater. These methods are not cost-effective at large scale, leads to the generation of secondary chemical sludge and are less effective when less concentration of heavy metal is present in the effluent. However, biosorption has been considered as an inexpensive and highly effective method for the removal of toxic heavy metal ions like Cr (VI), Cd (II) and Pb (II) from the liquid phase. A large number of biomaterials such as activated carbon, lignite, wheat grain husk, rice husk, banana peels, and nanoparticles have been utilized as biosorbents for the removal of heavy metal ions. Bacterial strains isolated from the contaminated site have also showed effective heavy metal removal property. White rot fungi like *Pleurotus florida* mushroom has emerging application in heavy metal removal due to its high tolerance property against toxic metal ions.

In the present work, iron ions were doped on the rice husk for adsorption-cum-reduction of lethal Cr (VI) to less toxic and partially soluble Cr (III). Energy dispersive X-ray analysis and X-ray photoelectric spectroscopy disclosed the effective doping of iron on rice husk and significant reduction of Cr (VI) into Cr (III). Physico-chemical analysis exhibited that the surface of iron doped rice husk was rough and in houses amino and hydroxyl moieties in majority together with high organic content. The maximum removal of Cr (VI) ions was observed in the acidic range as the value of point zero charge was 3.32. The study of dimensionless numbers( $\varphi$ ,  $N_k$  and  $\lambda$ ) disclosed that the Cr (VI) adsorption on iron coated rice

husk was principally controlled by diffusion. Only 1.32% and 0.18% deviation in experimental results was observed for undoped and iron doped rice husk, respectively in correlation plot of artificial neural network. The values of film and pore diffusivity coefficients along with Bangham's model study revealed that the biosorption was film diffusion limited for iron ions coated rice husks. The maximal removal of Cr (VI) was found to be 81.56 % for iron doped which was much higher than uncoated (43.28 %) rice husk. The iron doped rice husk had high regeneration capacity up to several cycles of simultaneous adsorption and desorption. Isotherm, kinetic and thermodynamic modeling revealed that adsorption of Cr (VI) ions on the surface of iron doped rice husk was multilayer, chemisorptive, spontaneous, endothermic and favourable.

In the next objective, chitosan coated MnO<sub>2</sub> nanoparticles were synthesized through green route using curcumin and *Citrus limetta* peel extract. X-ray photoelectron spectroscopic analysis of chromium loaded nanoparticles confirmed the biosorption of Cr (VI), Cd (II) and Pb (II) onto biosorbent surface. X-ray photoelectron spectroscopic analysis also revealed that most of the Cr (VI) ions were reduced to Cr (III) on the biosorbent surface. Scanning electron and transmission electron microscopic images showed that these nanoparticles were spherical in shape, crystalline, ranged from 14 to 24 nm in size. The Fourier-transform infrared spectroscopy analysis indicated hydroxyl, carboxyl and amino groups on its surface. The dynamic light scattering showed a size distribution of nanoparticles as  $299.50 \pm 25.32$  nm. High Brunauer- Emmett-Teller specific surface area ( $76.19 \text{ m}^2/\text{g}$ ) of these nanoparticles provided more active sites for binding of heavy metal ions. Energy dispersive X-ray and ultimate analysis indicated the presence of Mn, O, C, H, and N. These elements were the major components of these nanoparticles and confirmed the presence of chitosan on nanoparticle surface. Elemental mapping indicates to successful biosorption of Cr (VI), Cd (II) and Pb (II) on the surface of chitosan coated MnO<sub>2</sub> nanoparticles. The lower value of  $\text{pH}_{\text{zpc}}$  (3.17) proved

the suitability of acidic pH values for conducting biosorption experiments for Cr (VI) and pH above 3.17 was suitable for biosorption of Cd (II) and Pb (II). The study of biosorption dynamics by using dimensionless numbers for Cr (VI), Cd (II) and Pb (II) ions showed that biosorption was mixed diffusion and transfer controlled for single metal ion system as well as ternary metal ion system. The artificial neural network modeling has been performed to compare experimental and predicted values. It has been found that both the experimental and predicted values for biosorbent seemed to be in agreement with each other showing a high  $R^2$  value in the range of 0.95 - 0.99 for Cr (VI), Cd (II), Pb (II) ion in the single metal system and  $R^2$  was 0.88 in ternary metal ion system. In both single and ternary metal ion system, better goodness of fit of Freundlich isotherm ( $R^2 = 0.99$ ) for Cr (VI) biosorption revealed multilayer Cr (VI) biosorption on the heterogeneous surface. Langmuir isotherm ( $R^2 = 0.99$ ) best fitted in the Cd (II) and Pb (II) biosorption which indicated monolayer coverage of heavy metal ions on the homogeneous surface. Pseudo-second order ( $R^2 = 0.99$ ) (chemisorption) kinetics best fitted in Cr (VI), Cd (II) and Pb (II) biosorption in both single and ternary metal ion system. The thermodynamic study of Cr (VI), Cd (II) and Pb (II) biosorption of both single and ternary metal ion system showed that biosorption was endothermic and spontaneous and entropy driven. Chitosan coated MnO<sub>2</sub> nanoparticles showed high Cr (VI), Cd (II) and Pb (II) removal efficiency upto 92.19 %, 98.01 %, 94.40% at 100 mg/L initial metal ion solution and 1 g/L biosorbent dosage in a single metal ion system. In the ternary metal ion system, biosorbent was able to removal 53.90 % Cr (VI), 48.09 % Cd (II) and 57.96 % Pb (II) in the ternary metal ion system. Chitosan coated MnO<sub>2</sub> nanoparticles showed high regeneration capacity which could be used in several adsorption-desorption cycles.

In this objective, *Citrus limetta* was coated with chitosan polymer for removal of Cr (VI), Cd (II) and Pb (II). Energy dispersive X-ray and elemental mapping indicated the homogeneous distribution of Cr (VI), Pb (II) and Cd (II) together with other major elements

like carbon, nitrogen and oxygen which are considered as a major elemental constituent of chitosan and play a significant role in heavy metal biosorption as well as Cr (VI) biotransformation. The surface of the synthesized adsorbent was observed to be rough and porous.  $\text{pH}_{\text{zpc}}$  of chitosan coated *Citrus limetta* peel biomass was estimated as 3.69. Atomic force microscopy showed that the roughness of chitosan coated *Citrus limetta* peel biomass increased up to 146.62 nm as compared to uncoated one (28.62 nm). X-ray photoelectron spectroscopic analysis confirmed the biosorption of Cr (VI), Cd (II) and Pb (II) on the chitosan coated *Citrus limetta* peel biomass. The Fourier-transform infrared spectroscopy analysis indicated that functional groups such as hydroxyl, carboxyl and amino groups actively participated in the biosorption of Pb (II), Cd (II) and Cr (VI) onto chitosan coated *Citrus limetta* peel biomass. The dynamics of heavy metal biosorption onto chitosan coated *Citrus limetta* peel biomass was described by dimensionless numbers for both single ternary metal ion system which indicated that biosorption was mixed diffusion and transfer controlled. It was observed that both the experimental and predicted values for chitosan coated *Citrus limetta* peel biomass were consistent with each other, with high  $R^2$  values ranging from 0.92 to 0.99 for Cr (VI), Cd (II), and Pb (II) ion in single metal system and an  $R^2$  value of 0.86 for the ternary metal system was obtained. Freundlich isotherm ( $R^2 = 0.99$ ) isotherm model best fitted in biosorption data of Cr (VI) in both single and ternary metal ion system which indicates the multilayer biosorption of Cr (VI) onto heterogeneous chitosan coated *Citrus limetta* peels biomass. Langmuir isotherm was best fitted in the Cd (II) and Pb (II) biosorption in both single and ternary metal ion systems. Kinetic study indicated that pseudo second order kinetic model suitably fitted in the biosorption data of Cr (VI), Cd (II) and Pb (II) of both single and ternary metal ion systems. Thermodynamics indicated that Cr (VI) adsorption was spontaneous, endothermic and entropy driven. Results showed that chitosan coated *Citrus limetta* peels biomass has Cr (VI), Cd (II), and Pb (II) removal efficiency up to 99.34 % Cr (VI), 99.92 %

Cd (II), 99.58 % Pb (II) in single metal ion system and 56.19 % Cr (VI), 62.29 % Pb (II), 68.29 % Cd (II) in the ternary metal ion system at 100 mg/L initial metal ion concentration and 10 g/L chitosan coated *Citrus limetta* peels biomass. A combination of two batch reactors in series was capable in removing 100 % heavy metal ions in single and ternary metal ion system. Chitosan coated *Citrus limetta* peels biomass also showed high regeneration capacity and can be used over several biosorption cycles for the removal of Cd (II), Cr (VI) and Pb (II).

Also, a heavy metal tolerance bacteria was isolated from the wastewater collected from Baliya Nala (drain) Singrauli, Madhya Pradesh, India wherein coal mining units discharge their effluents after treatment. The bacterial isolate showed maximum sequence similarity with the *Microbacterium paraoxydans* and it was submitted to the NCBI GenBank under the accession no. MN650647. The bacterial isolate was named *Microbacterium paraoxydans* strain VSVM IIT (BHU) accession no. MN650647. The scanning electron microscopic and energy dispersive X-ray analysis indicated that the cells of the bacterial isolate which were grown in Luria-Bertani broth containing Cr (VI), Cd (II) and Pb (II) got enlarged after the bio-accumulation of heavy metal ions, whereas Si, O and C ions were observed on the cell surface. The Fourier-transform infrared spectroscopy indicated that several functional groups on the biosorbent surface participated in the biosorption of heavy metal ions. During the bacterial mediated adsorption, some portion of heavy metal ions accumulated in the bacterial cells and few metal ions bound to the bacterial surface and the presence of heavy metal in bacterial cells was confirmed through X-ray photoelectron spectroscopic. The optimum growth was observed at 37°C and pH 7. It was observed that the presence of both single and ternary metal ions in the solution enhanced the production of antioxidant enzymes such as glutathione S-transferase, catalase, superoxide dismutase and peroxidase within the cells. The concentration of these enzymes increased with the increase in heavy metal concentration in the growth medium. The study of heavy metal removal dynamics for bacteria using dimensionless numbers for Cr (VI),

Cd (II) and Pb (II) ions showed that biosorption was mixed diffusion and transfer controlled for single and ternary metal ion system based on the value of  $N_K$  ( $9.09 \times 10^{-3}$ ,  $9.83 \times 10^{-3}$  and  $9.32 \times 10^{-3}$  for Cr (VI), Cd (II) and Pb (II) ions in single metal ion system,  $9.49 \times 10^{-3}$ ,  $9.92 \times 10^{-3}$  and  $1.23 \times 10^{-2}$  for Cr (VI), Cd (II) and Pb (II) ions in ternary metal ion system. It has been found that both the experimental and predicted values for novel bacterial isolate seemed to be in agreement with each other showing a high  $R^2$  value in the range of 0.94 - 0.98 for Cr (VI), Cd (II), Pb (II) ions in single metal ion system and ternary metal ion system. The bacterial isolate showed a maximum heavy metal ion removal efficiency of 99.96 % Cr (VI), 94.96 % Pb (II), 84.96 % Cd (II) at 50 mg/L for single metal ion system and 91.62 % Cr (VI), 89.29 % Pb (II), 83.29 % Cd (II) at 50 mg/L of each metal ions in the ternary metal ion system.

Additionally, bioremediation of heavy metal ions from the coal washery effluent by *Pleurotus florida* was investigated. Metal ion concentration in the fruit body and substrate (paddy straw) was determined by inductively coupled plasma optical emission spectrometry. The fitness functions of exponential and linear extension growth models were evaluated mathematically (goodness of fit) at boundary conditions at  $t = 0$  and at  $t = t$ . The surface characterization of *Pleurotus florida* showed that the surface of *Pleurotus florida* was rough, heterogeneous in nature together with negatively charged functional groups like carboxyl, hydroxyl, ketonic and esters. The elemental composition of *Pleurotus florida* revealed the abundance of carbon and oxygen in biomass compared to other elements such as nitrogen and phosphorus. Growth modeling of *Pleurotus florida* revealed the fact that experimental and theoretical values of linear extension growth rate  $k_r$  ( $\text{mm d}^{-1}$ ) constant were not only close to each other but also they ranged from 1.36 to 2.21  $\text{mm d}^{-1}$  and 1.41 to 2.03  $\text{mm d}^{-1}$ . This showed the supremacy of the linear growth extension model over the exponential rate model. The metal toxicity stress markers like metallothionein (35.21  $\mu\text{g/g}$ ), superoxidase dismutase (9.4 U/mg), lipid peroxidase (2.5 nmol/mg), catalase (2.15 Pkat/mg) and reduced glutathione (28.09  $\mu\text{g/g}$ )

had higher level expression in the fruit bodies of *Pleurotus florida* grown in coal washery effluent as compared to control. The simultaneous increase of metallothionein concentration from 2.50 to 35.21  $\mu\text{g/g}$  with the increase in the concentration of metal ions in the term of CWE concentration (25 to 100%) in media showed the bioaccumulation of metal ions in the intracellular space. The maximum heavy metal uptake capacity of *Pleurotus florida* was found as 10.65, 1.12, 13.46, 3.0, 1.21, 19.11, 0.47 and 0.23 $\mu\text{g/g}$  for Pb, Cr, Cd, Zn, As, Mn, Ni and Ti, respectively. The maximum heavy metal removal from substrate (paddy straw) was found 99.53 % (Cd), 70.85 % (Cr), 77.77 % (Ni), 76.23 % (Zn), 42.63 % (Mn), 52.10 % (Pb), 49.07 % (Ti) and 51.66 % (As). The negatively charged rough surface, high amount of carbon and oxygen in biomass and the induced production of intracellular metal stress markers on exposure to heavy metals illustrated the immense bioaccumulation ability of *Pleurotus florida* in coal washery effluent.

On the basis of present work, we concluded that biosorbents developed were inexpensive, non-toxic and highly effective for the removal of hexavalent chromium, cadmium and lead. The LCA study for the removal of Cr (VI), Cd (II) and Pb (II) from contaminated wastewater helps to define the environmental impacts accompanying during handling, production, use, and recycling.